

Received: 4 May 2017

DOI: 10.1002/mop.30865

# Modeling of field dependent Maxwell-Wagner interfacial capacitance for bilayer metal-insulator-metal capacitors

D. Kannadassan | P. S. Mallick 

VIT University, Vellore 15, India

## Correspondence

P. S. Mallick, VIT University, Vellore-15, India.

Email: psmallick@vit.ac.in

## Abstract

In this letter, we have presented the modeling of field dependent Maxwell-Wagner interfacial capacitance for bilayer metal-insulator-metal (MIM) capacitors. The model was verified with measured capacitance-voltage characteristics of fabricated bilayer  $\text{Al}_2\text{O}_3/\text{TiO}_2$  MIM capacitors. The model reveals the origin of voltage linearity of MIM capacitors at low frequencies ( $<10$  kHz). The proposed model for bilayer/multilayer MIM capacitors is very useful tool to design circuits for mixed signal, analog and digital circuits with low variation of capacitance for change in voltage.

## KEYWORDS

anodization, frequency dependant capacitance, high- $k$ , MIM capacitor, voltage linearity

## 1 | INTRODUCTION

Metal-insulator-metal (MIM) capacitors are popular and attractive passive elements for analog and mixed signal (AMS) applications. MIM structures have weak dependence of capacitance with applied voltage since there is no oxide/oxide or oxide/semiconductor interface. This dependence is often referred as ‘voltage linearity’ or ‘voltage coefficient of capacitance (VCC)’. Some of the sensitive circuits, such as  $A/D$  converter ICs, expect a very low VCC of less than 100 ppm  $\text{V}^{-2}$  with high capacitance density and low leakage current density. Many dielectric materials were studied in the past decade to analyse the VCC, however, no single dielectric layer MIM capacitors could show such a low VCC till date. In this regard, various high- $k$  dielectric stack MIM

capacitors were proposed by many authors in recent days.<sup>1–4</sup> Although stacked MIM capacitors show low VCC at high frequencies, the frequency dependent voltage linearity reveals that VCC is very high about  $>10^4$  ppm  $\text{V}^{-2}$  at low frequencies.<sup>4</sup> Interfacial polarization or electrode polarization is assumed as origin of such increase in VCC as a result of field dependent permittivity.

Researchers have developed analytical or empirical models for voltage linearity using various micro and macroscopic polarization mechanisms in dielectrics, such as orientation polarization,<sup>4</sup> electrode polarization,<sup>5</sup> electrostriction,<sup>6</sup> and ionic polarization.<sup>7</sup> Recently, our group has demonstrated the modeling of voltage linearity of high- $k$  dielectric MIM capacitor using microscopic and macroscopic models of ionic and orientation polarization.<sup>8</sup> It is observed that required thickness increases with dielectric constant. This model predicts that the thickness of dielectric layer should be  $\sim 110$  nm for higher dielectric constant ( $>30$ ) to achieve VCC of 100 ppm  $\text{V}^{-2}$ . Although, this model shows a good agreement with experimental results at 100 MHz, it does not fit for VCCs at low frequencies. It is observed that the value of VCC is higher at low frequencies. This could be due to migration and accumulation of charges at the interface of dielectrics which is dominant at low frequencies. Such accumulated charges polarize for the applied field, such mechanism is referred as Maxwell-Wagner (MW) polarization.<sup>9</sup>

MW polarization is observed in many ferroelectric mixtures or heterostructures.<sup>10–14</sup> The accumulated charges at the interface of heterostructures for the applied field lead to the enhancement of effective permittivity. A giant dielectric constant of 1000 was achieved with ALD  $\text{TiO}_2/\text{Al}_2\text{O}_3$  nanolaminates by Li et al.<sup>15</sup> Because of MW polarization, the each  $\text{TiO}_2/\text{Al}_2\text{O}_3$  interface accumulation yields a high dielectric constant of 750 times greater than that of  $\text{Al}_2\text{O}_3$ . Recently, MW effect was found in MOS device by Jinesh et al.<sup>16</sup> It is worth to note that the MW charge accumulation is observed in forward bias only, i.e., the charge injection from high conductive semiconductor to low conductive high- $k$  material. The approach of imaginary permittivity  $\epsilon''$  to unity in forward bias at low frequencies indicates the presence of MW polarization.<sup>16</sup> However, models developed in these reports have ignored the dependence of applied potential across the dielectric stack.

Like single layer dielectrics MIM capacitors, modeling of capacitance-voltage characteristics of bilayer or multilayer MIM capacitors are not reported yet as per our knowledge. In this letter, we have developed a model for voltage dependence of bilayer dielectrics MIM capacitor using MW polarization. This model considers the carrier tunnelling probability of dielectric stack and MW relaxation time of accumulated interfacial charges. A good agreement was found between the model and the measured capacitance-

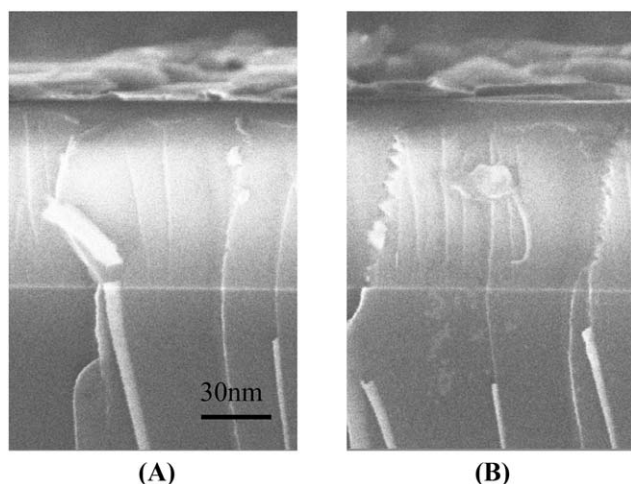


**FIGURE 1** SEM cross section image of anodized bilayer region before top electrode deposition, (A) sample A1: AV = 25 V, (B) sample A2 AV = 30 V

voltage characteristics of  $\text{TiO}_2/\text{Al}_2\text{O}_3$  MIM capacitors. It is observed that the MW polarization is significant in low frequencies of <10 kHz.

## 2 | FABRICATION AND CHARACTERIZATION

A 100 nm  $\text{SiO}_2$  isolation layer was grown on Si substrate and thoroughly cleaned by deionized water. Over that, a bilayer of 15 nm Ti on 100 nm Al is deposited using electron beam evaporator with tungsten filament at a pressure of  $8 \times 10^{-5}$  mBar. This Ti/Al film was anodized potentiostatically using nonaqueous solution of ammonium pentaborate dissolved in ethylene glycol ( $20 \text{ g l}^{-1}$ ) by the same size of platinum cathode. Oxidation was done for various anodization voltages of 15, 20, 25, and 30 V till the anodization current density reduces to  $1 \mu\text{A cm}^{-2}$ . Only three-quarters of sample area was dipped in the electrolyte to avoid etching for bottom electrode. This forms a barrier type anodic  $\text{TiO}_2$  and bilayer of  $\text{TiO}_2/\text{Al}_2\text{O}_3$  at lower and higher anodization voltages respectively. After cleaning thoroughly by deionized water, a 50 nm thick Al top electrode was deposited on the samples using thermal evaporation with the shadow mask area of  $0.61 \text{ mm}^2$ . Bilayer  $\text{TiO}_2/\text{Al}_2\text{O}_3$  MIM capacitors anodized at 25 and 30 V are named samples A1 and A2, respectively.

Scanning electron microscope (SEM) cross-section views of these sample are shown in Figure 1. The anodized secondary layer of  $\text{Al}_2\text{O}_3$  is visible between Anodized  $\text{TiO}_2$  and Al. The penetration depth was found about 2–3 nm. Figure 2 shows the depth profile of both samples using secondary ion mass spectrometry (SIMS) in positive mode with 1 kVCs. It shows ion distribution of Ti, Al, O, Si, Ti-O, and Al-O. At low anodization voltages (15 V and 20 V), Al bottom

electrode is also slightly anodized which was reported in Ref. [17]. This is due to outward migration of Al ion which forms a thin interface layer of AlTiO. At higher anodization voltages (25 V and 30 V), the inward migration of oxygen ion increases which forms a thin layer of  $\text{Al}_2\text{O}_3$ . It is observed that outward migration of Al into  $\text{TiO}_2$  is increased which increases the thickness of AlTiO composite layer. X-ray diffraction patterns of the samples are shown in Figure 3. It is observed that the crystalline phases of  $\text{TiO}_2$  anatase and rutile are present at low anodization voltages (<20 V). At higher anodization voltages, the crystalline  $\gamma\text{-Al}_2\text{O}_3$  emerges at  $2\theta = 65.5^\circ$ . Crystallization of anodic  $\text{TiO}_2$  has been addressed by many authors and summarized in our earlier work.<sup>17</sup> Readers are recommended to read the nucleation/crystallization of anodic bilayer oxides reported in Refs. [18] and [19].

The low frequency capacitance and leakage current density were measured using semiconductor parameter analyzer (HP4155C). The measured capacitance-voltage (CV) characteristics of samples A1 and A2 at 1, 5, and 10 kHz are shown in Figure 4. The CV characteristics are asymmetric and

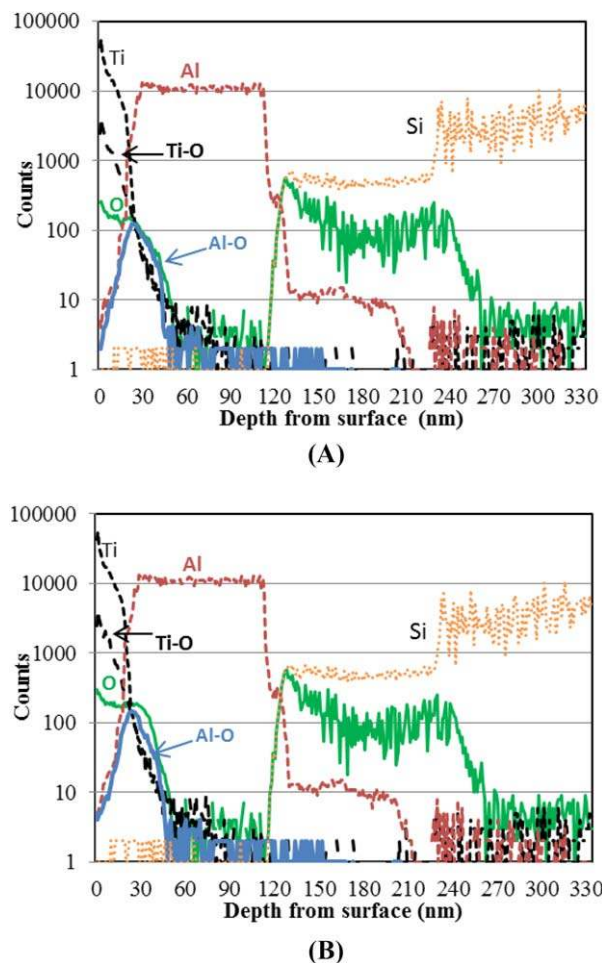


**FIGURE 2** SIMS depth profile: (A) sample A1: AV = 25 V, (B) sample A2 AV = 30 V. [Color figure can be viewed at [wileyonlinelibrary.com](http://wileyonlinelibrary.com)]

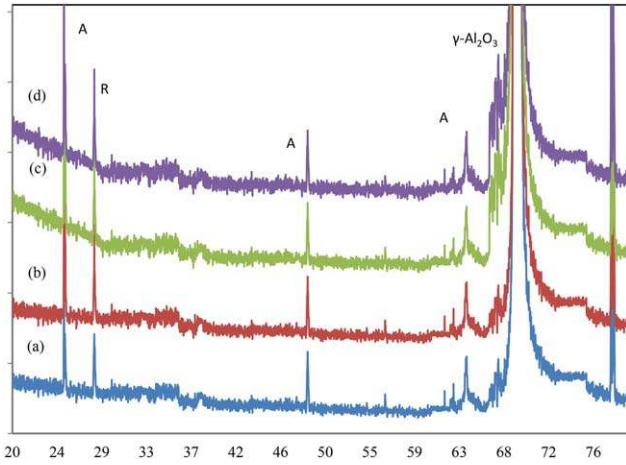


**FIGURE 3** X-ray diffraction spectra of anodized samples at various anodization voltages (A) 15 V, (B) 20 V, (C) 25 V, (D) 30 V (A: anatase, R: rutile). [Color figure can be viewed at wileyonlinelibrary.com]

frequency dependent. This is due to the accumulation of charges for reverse bias which enhances the capacitance. Also, the maximum capacitance at reverse bias decreases with increment in frequency. Figure 5 shows the measured leakage current density as a function of applied voltage at room temperature. It has been observed that both samples show a high degree of asymmetry between forward and reverse biases. This is due to the formation of AlTiO interfacial layer, TiO<sub>2</sub>/Al<sub>2</sub>O<sub>3</sub> stack and interfacial traps/charges. A detailed discussion of leakage characteristics and conduction mechanism of these bilayer MIM capacitors are reported in Ref. [20].

### 3 | VOLTAGE DEPENDENT MW CAPACITANCE MODEL

A bilayer MIM structure is considered as shown in Figure 6A. The layers consist of two dielectric materials with distinct relative dielectric constant of  $\epsilon_{r1}$  and  $\epsilon_{r2}$  with thickness of  $d_1$  and  $d_2$  respectively. Each layer's conductivity and relaxation time are represented as  $\sigma_n$  and  $\tau_n$ , respectively, for

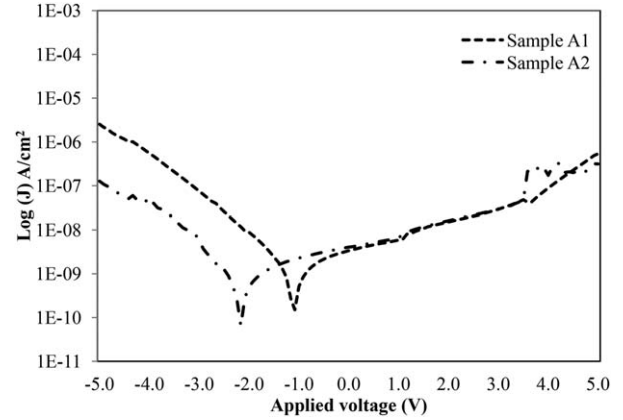


**FIGURE 5** Measured leakage characteristics of both samples at room temperature

$n = 1, 2$ . Figure 6B shows the equivalent RC network of bilayer MIM structure. Here  $R_1$  &  $C_1$  and  $R_2$  &  $C_2$  are individual resistance and capacitance of layer-1 and layer-2 respectively.  $C_{MW}$  is interfacial capacitance, also called MW capacitance, which is significant at low frequencies. The total capacitance can be expressed as:

$$C_{\text{tot}}(V_B) = \left( \frac{1}{C_1} + \frac{1}{C_2} \right)^{-1} + C_{MW}(V_B) \quad (1)$$

where MW capacitance can be calculated by

$$C_{MW} = Aq^2 N_{MW} \quad (2)$$

Here  $q$  is charge of an electron and  $A$  is top electrode area of capacitor.  $N_{MW}$  is the accumulated charge density at the interface for the applied bias voltage  $V_B$ . According to MW theory of double layer,<sup>21,22</sup> the accumulated charge density at the interface as a function of applied potential and time is expressed as:

$$N_{MW} = \epsilon_0 \left[ \frac{(\epsilon_{r1}\sigma_2 - \epsilon_{r2}\sigma_1)}{(\sigma_1 d_2 + \sigma_2 d_1)} \right] \cdot V_{\text{stack}} \cdot \left[ 1 - e^{-\frac{t}{\tau_{MW}}} \right], \quad (3)$$

Here  $V_{\text{stack}}$  is voltage across the bilayer dielectric stack for the applied bias voltage  $V_B$ ,  $t$  is time period of

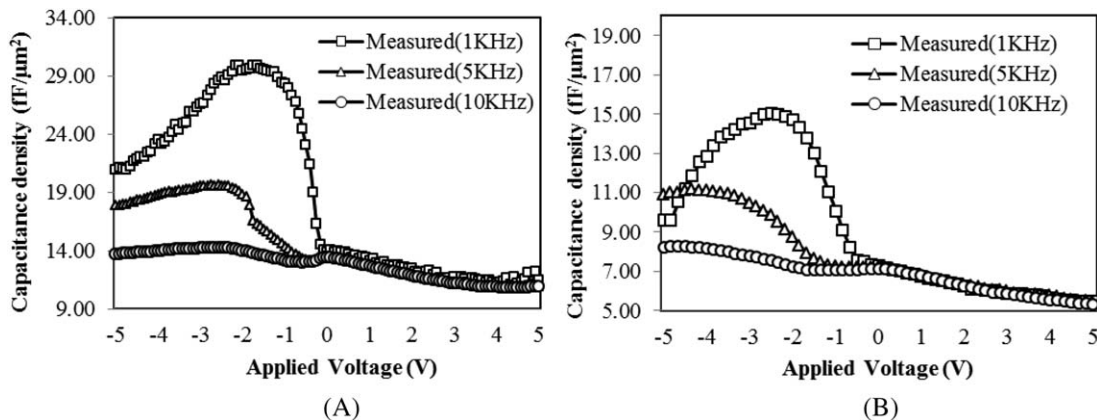


**FIGURE 4** Measured capacitance voltage characteristics for low frequencies at room temperature: (A) sample A1 and (B) sample A2

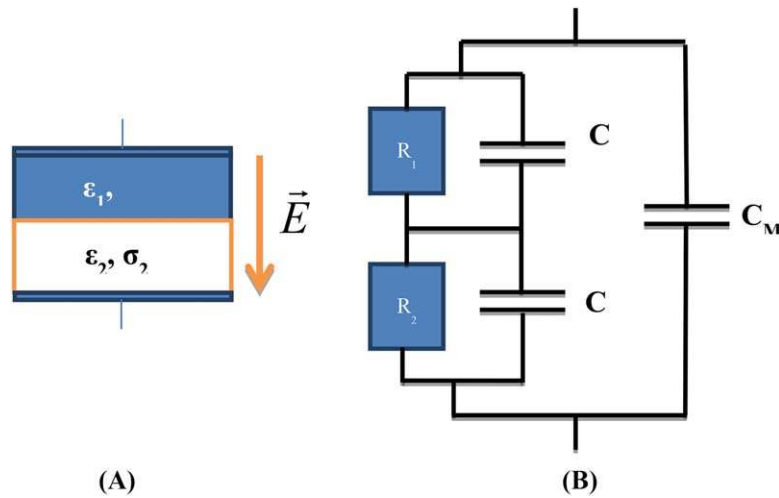


**FIGURE 6** Schematic of bilayer configuration: (A) layer specification, (B) equivalent circuit at low frequencies. [Color figure can be viewed at wileyonlinelibrary.com]

**TABLE 1** Fitting parameters of Maxwell-Wagner capacitance model

Sample name	$d_1$ (nm)	$d_2$ (nm)	$\epsilon_{r1}$	$\epsilon_{r2}$	$\sigma_1$ (pS cm <sup>-1</sup> )	$\sigma_2$ (pS cm <sup>-1</sup> )	$\phi_1$ (eV)	$\phi_2$ (eV)	$V_{bi}$ (V)
A1	15	7	90	9	15	$2 \times 10^{-3}$	3.3	2.3	1
A2	15	10	90	9	15	$2 \times 10^{-3}$	3.3	2.3	1.2

measurement or time period of the one full cycle of AC signal, and  $\tau_{MW}$  is relaxation time of double layer. The accumulated interface charges and native traps built up potential which opposes the applied field and reduces flow of charges, so the potential across stack can be written as  $V_{stack} = |V_B - V_{bi}|$ . Here  $V_{bi}$  is built in potential at interface. MW time constant can be expressed as

$$\tau_{MW} = \frac{d_1 \epsilon_2 + d_2 \epsilon_1}{\sigma_1 d_2 + \sigma_2 d_1} \quad (4)$$

If the measurement time/period of the cycle  $t$  is very greater than  $\tau_{MW}$ , then the third term of eq. 3 can be eliminated. Therefore, we shall rewrite eq. 3 as:

$$N_{MW} = \frac{\sigma_1 \sigma_2 \left( \frac{\epsilon_1}{\sigma_1} - \frac{\epsilon_2}{\sigma_2} \right)}{d_1 d_2 \left( \frac{\sigma_1}{d_1} + \frac{\sigma_2}{d_2} \right)} \cdot |V_B - V_{bi}| \quad (5)$$

We know  $\tau_1 = \frac{\epsilon_1}{\sigma_1}$  and  $\tau_2 = \frac{\epsilon_2}{\sigma_2}$ . Conductance  $G_1 = \frac{1}{R_1} = \frac{\sigma_1}{d_1}$  and  $G_2 = \frac{1}{R_2} = \frac{\sigma_2}{d_2}$ . By substituting these expression in eq. 3

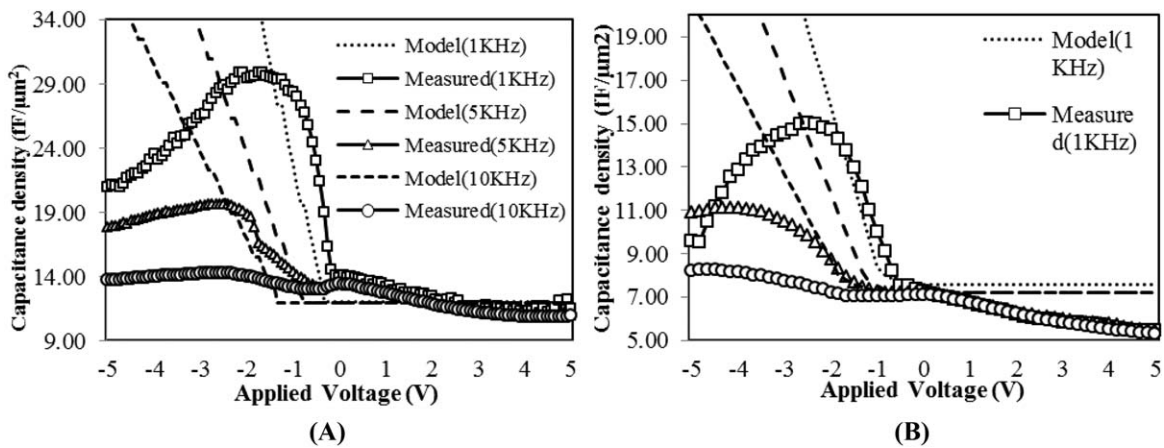


**FIGURE 7** MW capacitance voltage model (without tunneling probability) and measured C-V fitting compatibility for samples (A) AT-3 and (B) AT-4

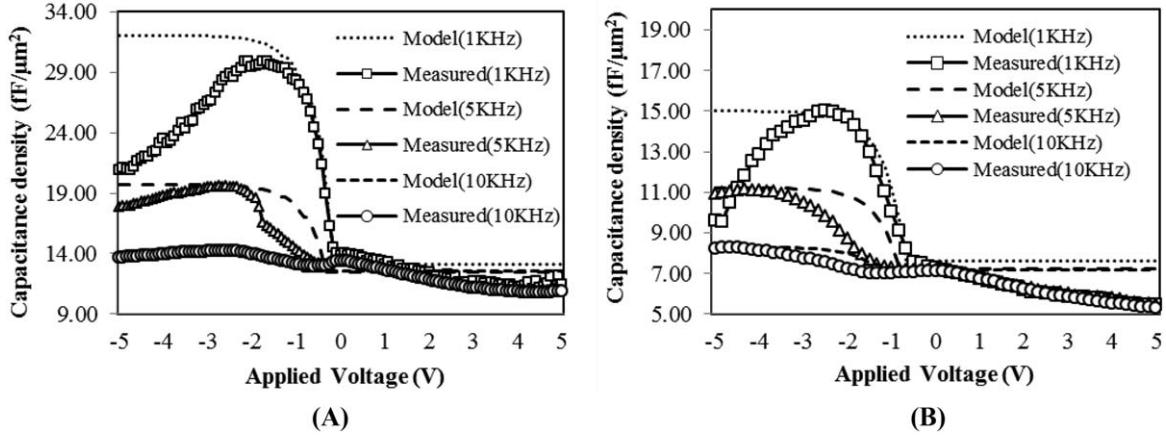


**FIGURE 8** MW capacitance voltage model (with tunneling probability) and measured C-V fitting compatibility for samples: (A) AT-3 and (B) AT-4

$$N_{MW} = \left( \frac{G_1 G_2}{G_1 + G_2} \right) \cdot (\tau_1 - \tau_2) \cdot |V_B - V_{bi}| = G \cdot (\tau_1 - \tau_2) \cdot |V_B - V_{bi}| \quad (6)$$

Since, two conductance are in series,  $G = \frac{G_1 G_2}{G_1 + G_2}$ . On the other hand, imaginary part of dielectric permittivity is expressed as:<sup>12</sup>

$$\epsilon'' = \frac{1 + \omega^2 [(\tau_{MW} \cdot \tau_1) + (\tau_{MW} \cdot \tau_2) - (\tau_1 \cdot \tau_2)]}{\omega C_0 (R_1 + R_2) (1 + \omega^2 \tau_{MW}^2)} \quad (7)$$

and  $G = \omega C_0 \epsilon''$ .  $C_0$  is the capacitance at no applied voltage. Thus, the eq. 5 can be written as:

$$N_{MW} = \frac{1 + \omega^2 [(\tau_{MW} \cdot \tau_1) + (\tau_{MW} \cdot \tau_2) - (\tau_1 \cdot \tau_2)]}{\omega C_0 (R_1 + R_2) (1 + \omega^2 \tau_{MW}^2)} \cdot (\tau_1 - \tau_2) \cdot |V_B - V_{bi}| \quad (8)$$

The above equation describes the quantity of accumulated charges according to the MW theory. The parameters are assumed and calculated to validate this model as shown in Table 1. The model is accounted only for reverse and forward bias that considered as voltage independent. The compatibility of proposed model with measured capacitance for the applied voltages at various frequencies is shown in Figure 7A and B for samples A1 and A2, respectively. It is clear that the model is not fitting with measured C-V characteristics. This is due the linear relation of applied voltage with accumulated charge density as shown in eq. 8. This also reveals that charge migration between dielectric materials is ignored.

To incorporate realistic situation, tunnelling probability has been added with existing model based on Poole-Frenkle emission model.<sup>23</sup> Therefore, eq. 8 can be rewritten as:

$$N_{MW} = \frac{1 + \omega^2 [(\tau_{MW} \cdot \tau_1) + (\tau_{MW} \cdot \tau_2) - (\tau_1 \cdot \tau_2)]}{\omega C_0 (R_1 + R_2) (1 + \omega^2 \tau_{MW}^2)} \cdot (\tau_1 - \tau_2) \cdot |V_B - V_{bi}| \left\{ 1 - \exp \left( \frac{(qV_{stack} - \phi_1 + \phi_2)}{kT} \right) \right\} \quad (9)$$

In this model,  $\phi_1$  and  $\phi_2$  are barrier potentials of dielectric layers. Table 1 shows the value of these potentials. Fitting compatibility of this proposed model with measured data is shown in Figure 8A and B. A close fit of model with tunneling probability is observed. Unlike high frequencies, the low frequency capacitance shows a striking asymmetry between forward and reverse biases. This similar asymmetric property was also observed in leakage characteristics of bilayer capacitors. This indicates the positive traps/charges are not only sensitive to temperature, but also with the applied electric field direction and frequency of input AC signal. The polarization and accumulation of interface charges between two distinct dielectric materials are referred as MW polarization.

MW effect of permittivity enhancement in bilayer MIM capacitors leads to increase in VCC at low frequencies. It is observed that the ratio of permittivity of both dielectric material ( $R_{di} = \frac{\epsilon_{d1}}{\epsilon_{d2}}$ ) largely determines VCC which is responsible for MW capacitance. For instance,  $TiO_2/Al_2O_3$  has  $R_{di} = 90/9 = 10$  which shows a capacitance enhancement of twice compared to series capacitance of bilayer in our experiments. At the same time, sandwich of  $TiO_2$  and  $Al_2O_3$  multilayer stack shows a giant dielectric constant of  $>500$  times of single layer MIM structure.<sup>15</sup> Therefore, the dependence of capacitance with voltage can be reduced by choosing the materials with less  $R_{di}$ , such as  $ZrO_2/HfO_2$  ( $29/25 = 1.16$ ) and  $HfO_2/Al_2O_3$  ( $29/9 = 3.22$ ).

## 4 | CONCLUSIONS

This article reveals the origin of low frequency VCC of bilayer/multilayer MIM capacitors. Field dependent capacitance of bilayer MIM capacitors is deduced from Maxwell approach on accumulation of charges at dielectric interface. The voltage dependence of dielectric enhancement can be modeled with Wagner equation on space charge polarization. The model shows good agreement with experiment and

confirms that the MW polarization occurs at low frequencies and largely depends on field direction. The charge built-up due to tunneling and accumulation has added more accuracy compared to ideal case. The model helps in selection of materials and design of low VCC MIM capacitors for highly sensitive applications such as medical devices and signal processing units.

## ACKNOWLEDGMENTS

The authors would like to acknowledge financial support by Indian Nanoelectronics User's Program (INUP), Government of India, through Center for Excellence in Nanoelectronics, IIT-Bombay. Authors also would like to thank Prof. A. Q. Contractor and Dr. K. Nageswari of IIT-Bombay for their support.

## ORCID

P. S. Mallick  <http://orcid.org/0000-0002-9047-9507>

## REFERENCES

- [1] Kaynak M, Lukosius C, Costina B, et al. *Thin Solid Films*. 2011;519:734–739.
- [2] Wu J, Wu Y, Lin C, et al. *IEEE Electron Device Lett*. 2012;33(6):878–880.
- [3] Wu Y-H, Ou W-Y, Lin C-C, Wu J-R, Wu M-L, Chen L-L. *IEEE Electron Device Lett*. 2012;33(1):104–106.
- [4] Tsui HH, B, Cheng C. *IEEE Electron Device Lett*. 2010;31(8):875–877.
- [5] Gonon P, Vallae C. *Appl Phys Lett*. 2007;90(14).
- [6] Wenger C, Lupina G, Lukosius M, et al. *J Appl Phys*. 2008;103(10).
- [7] Be'cu S, Cre'mer S, Autran J. *Microelectron Eng*. 2006;83(11–12):2422–2426.
- [8] Kannadassan D, Karthik R, Shojaei Baghini M, Mallick P. *Solid-State Electron*. 2014;91:112–117.
- [9] Sillars R. *J Inst Electr Eng*. 1937;80(484):378–394.
- [10] Erbil Y, Kim RA. Gerhardt. *Phys Rev Lett*. 1996;77:1629.
- [11] Qu D, Evstigneev M, Johnson DJ, Prince RH. *Appl Phys Lett*. 1998;72(11):1394–1396.
- [12] O'neill R, Bowman M, Gregg JM. *Appl Phys Lett*. 2000;77(10):1520–1522.
- [13] Catalan G, O'neill D, Bowman RM, Gregg JM. *Appl Phys Lett*. 2000;77(19):3078–3080.
- [14] Shen M, Ge S, Cao W. *J Phys D: Appl Phys*. 2001;34(19):2935–2938.
- [15] Li W, Auciello O, Premnath RN, Kabius B. *Appl Phys Lett*. 2010;96(16).
- [16] Jinesh KB, Lamy Y, Klootwijk JH, Besling WFA. *Appl Phys Lett*. 2009;95(12).
- [17] Kannadassan D, Karthik R, Baghini MS, Mallick PS. *Mater Sci Semicond Process*. 2013;16(2).
- [18] Shimizu K, Kobayashi K, Skeldon P, Thompson G, Wood G. *Thin Solid Films*. 1997;295(1–2):156–161.
- [19] Yao L, Hua Liu J, Yu M, Li S. M, Wu H. *Trans Nonferrous Metals Soc China*. 2010;20(5):825–830.
- [20] Karthik R, Kannadassan D, Baghini M, Mallick P. *J Nanosci Nanotechnol*. 2013;13(10):6894–6899.
- [21] Maxwell JC. *A Treatise on Electricity and Magnetism*. Oxford: Clarendon Press; 1873.
- [22] Morshuis PHF, Bodega R, Fabiani D, Montanari G, Dissado LA, Smit J. *IEEE Int Conf Solid Dielectr*. 2007;450–453.
- [23] Houssa M, Tuominen M, Naili M, et al. *J Appl Phys*. 2000;87(12):8615–8620.

**How to cite this article:** Kannadassan D, Mallick PS. Modeling of field dependent Maxwell-Wagner interfacial capacitance for bilayer metal-insulator-metal capacitors. *Microw Opt Technol Lett*. 2017;59:2965–2970. <https://doi.org/10.1002/mop.30865>

Received: 4 May 2017

DOI: 10.1002/mop.30864

# Adjustable compact dual-band microstrip bandpass filter using T-shaped resonators

Shiva Khani<sup>1</sup>  |

Syed Vahab AL-Din Makki<sup>2</sup> |

Syed Mohammad Hadi Mousavi<sup>3</sup> |

Mohammad Danaie<sup>1</sup> | Pejman Rezaei<sup>1</sup>

<sup>1</sup> Faculty of Electrical and computer Engineering, Semnan University, Semnan, Iran

<sup>2</sup> Electrical Engineering, Faculty of Engineering, Razi University, Kermanshah, Iran

<sup>3</sup> Young Researchers and Elite Club, Hamedan Branch, Islamic Azad University, Hamedan, Iran

## Correspondence

Shiva Khani, Faculty of Electrical and computer Engineering, Semnan University, Semnan, Iran.

Email: shiva.khani@semnan.ac.ir

## Funding information

This work was supported by Semnan University.

## Abstract

In this letter, a compact dual-band bandpass filter (BPF) is designed, analyzed, and fabricated. A loop resonator